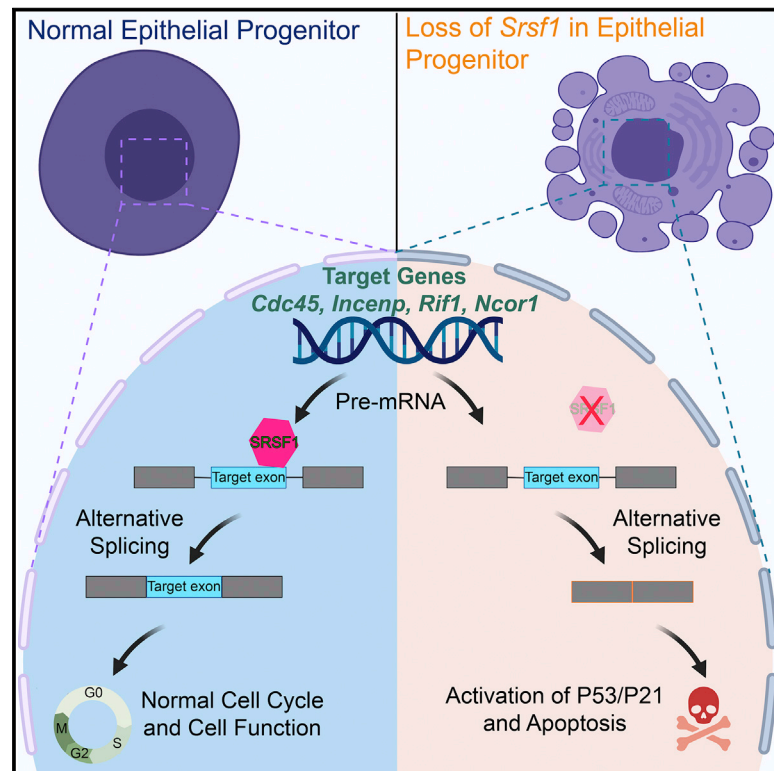


Developmental Cell

SRSF1 governs progenitor-specific alternative splicing to maintain adult epithelial tissue homeostasis and renewal

Graphical abstract



Authors

Tingsheng Yu, Oscar Cazares, Alison D. Tang, ..., Han-Sung Jung, Angela N. Brooks, Ophir D. Klein

Correspondence

ophir.klein@ucsf.edu

In brief

Cycling progenitors generate the terminally differentiated cells needed to maintain a functional organ. Yu et al. demonstrate in two self-renewing tissues, the ever-growing mouse incisor and the small intestine, that epithelial progenitors are maintained through proper splicing of several targets of the splice factor SRSF1.

Highlights

- SRSF1 governs epithelial progenitor homeostasis
- Mis-splicing of SRSF1 targets leads to epithelial progenitor cell death
- *Cdc45*, *Incenp*, *Rif1*, and *Ncor1* are important targets of SRSF1



Article

SRSF1 governs progenitor-specific alternative splicing to maintain adult epithelial tissue homeostasis and renewal

Tingsheng Yu,^{1,7} Oscar Cazares,^{1,7} Alison D. Tang,² Hyun-Yi Kim,³ Tomas Wald,¹ Adya Verma,¹ Qi Liu,⁴ Mary Helen Barcellos-Hoff,⁴ Stephen N. Floor,⁵ Han-Sung Jung,³ Angela N. Brooks,² and Ophir D. Klein^{1,6,8,*}

¹Department of Orofacial Sciences and Program in Craniofacial Biology, University of California, San Francisco, San Francisco, CA 94143, USA

²Department of Biomolecular Engineering, University of California, Santa Cruz, Santa Cruz, CA 95064, USA

³Division in Anatomy and Developmental Biology, Department of Oral Biology, Oral Science Research Center, BK21 PLUS Project, Yonsei University College of Dentistry, Seoul, Korea

⁴Department of Radiation Oncology, Helen Diller Family Comprehensive Cancer Center, University of California, San Francisco, San Francisco, CA 94115, USA

⁵Department of Cell and Tissue Biology, University of California, San Francisco, San Francisco, CA 94143, USA

⁶Department of Pediatrics and Institute for Human Genetics, University of California, San Francisco, San Francisco, CA 94143, USA

⁷These authors contributed equally

⁸Lead contact

*Correspondence: ophir.klein@ucsf.edu

<https://doi.org/10.1016/j.devcel.2022.01.011>

SUMMARY

Alternative splicing generates distinct mRNA variants and is essential for development, homeostasis, and renewal. Proteins of the serine/arginine (SR)-rich splicing factor family are major splicing regulators that are broadly required for organ development as well as cell and organism viability. However, how these proteins support adult organ function remains largely unknown. Here, we used the continuously growing mouse incisor as a model to dissect the functions of the prototypical SR family protein SRSF1 during tissue homeostasis and renewal. We identified an SRSF1-governed alternative splicing network that is specifically required for dental proliferation and survival of progenitors but dispensable for the viability of differentiated cells. We also observed a similar progenitor-specific role of SRSF1 in the small intestinal epithelium, indicating a conserved function of SRSF1 across adult epithelial tissues. Thus, our findings define a regulatory mechanism by which SRSF1 specifically controls progenitor-specific alternative splicing events to support adult tissue homeostasis and renewal.

INTRODUCTION

Alternative splicing generates mRNA variants through selective inclusion or exclusion of exons or introns during pre-mRNA processing. This process is the primary mechanism to increase the diversity of protein isoforms that are structurally and functionally specialized in different tissues to ensure normal development (reviewed in [Jin et al., 2018](#)). Over the past decade, transcriptomic analyses performed in individual organs or whole organisms have identified distinct clusters of alternative splicing events that are required in various cell populations, as well as at different developmental stages to support cell viability and tissue development ([Salomonis et al., 2010](#); [Graveley et al., 2011](#); [Zhang et al., 2014](#)). However, the spatial and temporal regulation of alternative splicing events by splicing regulators remains relatively unexplored. One mechanism for precisely controlling alternative splicing is via specific expression of splicing regulators in certain cell types ([Hayakawa-Yano et al., 2017](#)) or at

specific developmental stages ([Kalsotra et al., 2008](#)). However, because many splicing regulators are broadly expressed ([Kalsotra et al., 2008](#); [Yeo et al., 2009](#); [Damianov and Black, 2010](#)), additional mechanisms that confer specificity on these important RNA binding proteins must exist.

Among the principal regulators of alternative splicing are members of the serine/arginine (SR)-rich splicing factor family, which bind to splicing enhancer sequences to promote alternative splicing (reviewed in [Shepard and Hertel, 2009](#)). The SR splicing factor family has 12 members in humans that share a conserved SR domain (reviewed in [Manley and Krainer, 2010](#)). Many SR splicing factors have been reported to be essential for development. Germline deletion of these factors leads to embryonic lethality or perinatal death ([Jumaa et al., 1999](#); [Ding et al., 2004](#); [Xu et al., 2005](#); [Feng et al., 2009](#)), and tissue-specific deletion of SR genes causes organ failure, resulting in growth retardation and often lethality ([Xu et al., 2005](#); [Cheng et al., 2016](#)). Despite the indispensable role of SR splicing factors during early



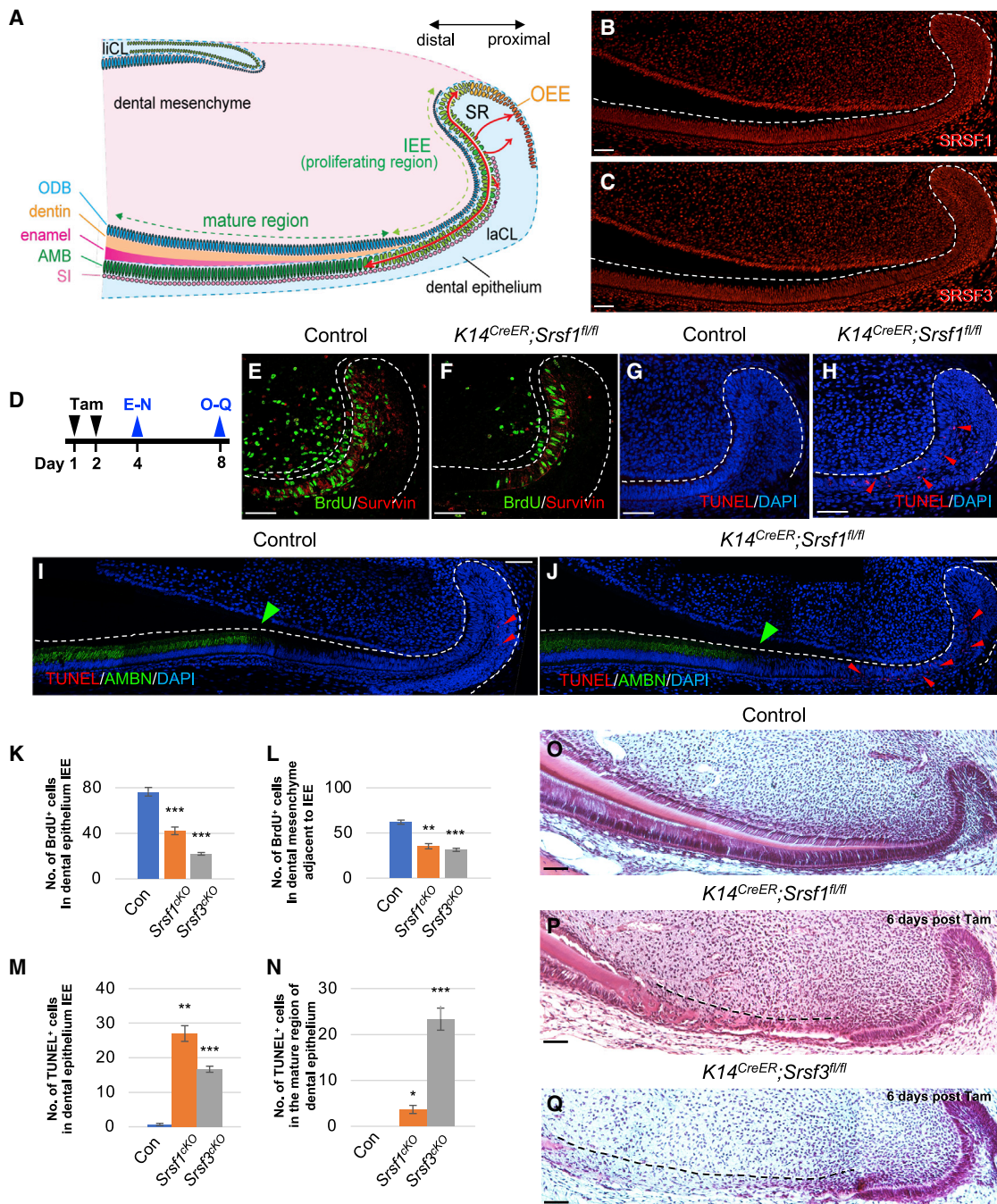


Figure 1. Deleting *Srsf1* specifically disrupts the function of dental progenitors in the adult mouse laCL

(A) Schematic diagram of the labial cervical loop (laCL), located at the proximal mouse incisor. Dental progenitors residing in the proliferating inner enamel epithelium (IEE) drive the formation and differentiation of a variety of cell types (red arrow lines), including the enamel-secreting ameloblasts (AMB), stellate intermedium (SI) cells, and other cell populations that reside in the outer enamel epithelium (OEE) and stellate reticulum (SR). Dental mesenchyme-derived odontoblasts (ODB) produce dentin at the lingual surface of enamel. liCL, lingual cervical loop. Light green dashed line with arrowheads marks the IEE region. Dark green dashed line with arrowheads marks the mature region.

(B and C) Immunostaining of SRSF1 (B) and SRSF3 (C) in the laCL.

(D) Timeline depicting tamoxifen (Tam)-induced Cre activation (black arrowheads) and sample collection (blue arrowheads).

(E and F) BrdU/survivin co-labeling in the control (E) and $K14^{CreER};Srsf1^{fl/fl}$ (F) laCL. White dashed lines with arrowheads outline the reduced region of proliferation in $K14^{CreER};Srsf1^{fl/fl}$ (F), compared with control (E).

(G and H) TUNEL staining in the control (G) and $K14^{CreER};Srsf1^{fl/fl}$ (H) laCL. Increased cell death (red arrowheads) was detected specifically in the proliferating IEE upon *Srsf1* deletion (H).

(legend continued on next page)

development, their functions in adult tissues are largely unknown. With more than 95% of genes undergoing alternative splicing in adult tissues (Pan et al., 2008; Wang et al., 2008), many important questions remain unanswered, including how SR splicing factors maintain tissue homeostasis and renewal, as well as their roles in various cell types, including stem cells, transit-amplifying progenitors, and differentiated cells.

We have turned to the continuously growing adult mouse incisor as a model to study the cellular function of SR splicing factors. The constant wear on the incisor as the animal gnaws on food is balanced by rapid replacement of cells and mineralized tissues, thanks to a pool of adult stem cells. Therefore, like other high turnover epithelial organs, such as the intestine, the balance between cell proliferation and differentiation must be maintained to ensure proper homeostasis and renewal. An epithelial structure located at the proximal end of the adult mouse incisor called the labial cervical loop (laCL) houses a group of proliferating progenitors that produce multiple cell populations to support the continuously growing incisors throughout the animal's lifetime (Figure 1A) (reviewed in Yu and Klein, 2020). Dental progenitors reside in the inner enamel epithelium (IEE), giving rise to multiple cell lineages, including those in the stellate reticulum and the outer enamel epithelium (OEE) regions at the proximal end of laCL. IEE progenitors also contribute to the differentiation and maturation of enamel-secreting ameloblasts and to the formation of a single layer of stratum intermedium cells immediately adjacent to the ameloblasts.

Here, we identify a regulatory mechanism by which the ubiquitously expressed SRSF1 protein specifically controls progenitor-specific alternative splicing events to maintain adult dental tissue homeostasis and renewal. Misregulation of the SRSF1-dependent splicing network activates the p53/p21 pathway, which arrests the cell cycle and impairs cell survival in the adult mouse laCL. Notably, a similar progenitor-specific function of SRSF1 is also observed in the small intestine epithelium, indicating a conserved role of SR splicing factors in regulating alternative splicing in adult epithelial tissues.

RESULTS

SRSF1 is required for maintenance of dental progenitors but dispensable in differentiated cell populations in the adult mouse incisor

We found that 11 SR genes were expressed in the adult mouse laCL (Figure S1A). In addition, our previous analysis suggested that *Srsf3* is highly expressed in the proliferating IEE cells of the laCL (Seidel et al., 2017), pointing to a role for SR splicing factors

in proliferative cells in this region. Furthermore, extensive autoregulation and cross-regulation have been reported among different SR splicing factors, especially between SRSF1 and SRSF3 (Ni et al., 2007; Gonçalves et al., 2009). Therefore, to better understand the role of SR splicing factors in adult tissue, we set out to study the cellular and regulatory mechanism of SRSF1 and SRSF3 in regulating adult mouse incisor homeostasis and renewal. We first performed immunostaining with amplification (Figures 1B, 1C, S1B, and S1C) and quantitative RNAscope *in situ* hybridization (Figures S1D–S1E'') to determine the expression patterns of SRSF1 and SRSF3 in the adult mouse laCL at high resolution. These analyses demonstrated that both SR splicing factors were ubiquitously expressed in the wild-type laCL.

To determine the cellular functions of SR splicing factors in the dental epithelium, we genetically deleted *Srsf1* or *Srsf3* in the adult incisor epithelium by crossing *Srsf1* (*Srsf1^{fl/fl}*) (Xu et al., 2005) or *Srsf3* (*Srsf3^{fl/fl}*) (Jumaa et al., 1999) conditional alleles with an inducible recombinase expressed in the epithelium, *Keratin 14^{CreER}* (*K14^{CreER}*) (Li et al., 2000). After two consecutive doses of tamoxifen injection (Figure 1D), Cre recombinase was induced in the incisor epithelium of *K14^{CreER};Srsf1^{fl/fl}* and *K14^{CreER};Srsf3^{fl/fl}* conditional knockout mutants, and this resulted in a loss of SRSF1 or SRSF3 protein, respectively, as shown by immunostaining (Figures S2A–S2D'', S3A, and S3B).

The impact upon deletion of SR genes was apparent 2 days after tamoxifen injection. Both proliferation and survival of dental progenitors in the *K14^{CreER};Srsf1^{fl/fl}* and *K14^{CreER};Srsf3^{fl/fl}* mutants were strongly disrupted. The number of 5-bromo-2'-deoxyuridine (BrdU⁺) cells was significantly reduced in the surviving co-labeled proliferating IEE region (Figures 1E, 1F, 1K, S3C, and S3F). A decrease in the number of BrdU⁺ progenitors was also observed in the dental mesenchyme adjacent to IEE in both mutants (Figures 1E, 1F, 1L, S3C, S3F), most likely resulting from mesenchymal-epithelial cross-talk. In addition, the number of TUNEL⁺ apoptotic cells was increased in the proliferating IEE region (Figures 1G–1J, 1M, S3D, and S3G). In the *K14^{CreER};Srsf3^{fl/fl}* mutant laCL, cell death was also detected in the differentiating and differentiated regions, including pre-ameloblasts and ameloblasts (Figures 1N, S3D, and S3G). In contrast, very low numbers of TUNEL⁺ cells were observed in the mature region of *K14^{CreER};Srsf1^{fl/fl}* dental epithelium (Figures 1I, 1J, and 1N). Furthermore, although the expression of the mature ameloblast marker ameloblastin (AMBN) was almost undetectable in *K14^{CreER};Srsf3^{fl/fl}* mutant dental epithelium (Figures S3E and S3H), the expression pattern of AMBN remained similar in both control and *K14^{CreER};Srsf1^{fl/fl}* mutant (Figures 1I and 1J). Disruption of the ameloblast layer with *Srsf3* deletion resulted in a lack of

(I and J) Co-labeling of TUNEL and immunostaining of AMBN in control (I) and *K14^{CreER};Srsf1^{fl/fl}* (J) laCL. Normal initiation and pattern of AMBN expression (green arrowheads) in both control (I) and *K14^{CreER};Srsf1^{fl/fl}* (J). Increased cell death (red arrowheads) was detected specifically in the proliferating IEE, and no TUNEL⁺ cells were detected in the mature region with AMBN expression upon *Srsf1* deletion (J). Images were stitched manually, selecting a common feature appearing in the overlapping region. A black background was applied to the top edges of the image to make up the gaps due to image stitching.

(K–N) Quantification of the number of BrdU⁺ cells in dental epithelium (K) and mesenchyme adjacent to IEE (L), TUNEL⁺ cells in the proliferating IEE region (M), and mature region (N) in the control (Con), *K14^{CreER};Srsf1^{fl/fl}* (*Srsf1^{cKO}*), and *K14^{CreER};Srsf3^{fl/fl}* (*Srsf3^{cKO}*) laCL. All quantitative data are shown as mean ± SD (*p < 0.05, ** p < 0.001, and *** p < 0.001).

(O–Q) H&E staining of the control (O), *K14^{CreER};Srsf1^{fl/fl}* (P), and *K14^{CreER};Srsf3^{fl/fl}* (Q) laCL 6 days after tamoxifen treatment. Black dashed lines with arrowheads outline the region of tissue damage in (P) and (Q) upon *Srsf1* (P) and *Srsf3* (Q) deletion, respectively. Images were stitched manually, selecting a common feature appearing in the overlapping region. Dashed lines outline laCL. Representative images and quantitative data are shown. Scale bar, 50 μm. See also Figures S1, S2, S3, and S7.

enamel formation (Figure S3K), compared with the orderly aligned ameloblasts and enamel mineralization in control (Figure S3I) and $K14^{CreER};Srsf1^{fl/fl}$ mutant (Figure S3J). These data suggest that SRSF1 and SRSF3 have intrinsically different roles in regulating ameloblast maturation.

Six days after tamoxifen injection, the $K14^{CreER};Srsf3^{fl/fl}$ mutant epithelium exhibited a much more severe loss of dental epithelial tissue (Figure 1P) compared with the $K14^{CreER};Srsf1^{fl/fl}$ mutants (Figure 1O), consistent with the larger number of affected cells in the $K14^{CreER};Srsf3^{fl/fl}$ mutants. Because of the rapid tissue turnover, the IEE had almost fully recovered in both mutants over this time period. Therefore, the regenerated IEE cells pushed the earlier affected tissue to a more distal region (Figures 1P and 1Q). Both $K14^{CreER};Srsf1^{fl/fl}$ and $K14^{CreER};Srsf3^{fl/fl}$ mutant animals ceased eating and became moribund 7 days after Cre induction, potentially due to the requirement for SR proteins in other epithelial organs, which precluded assessment of long-term consequences of *Srsf1* or *Srsf3* deletions.

These findings indicate that, despite both SR proteins showing ubiquitous expression patterns, they have distinct roles. SRSF3 is required in various cell types regardless of their cycling status. In contrast, SRSF1 displays a progenitor-specific function, and it is dispensable in differentiated cells. Given the specific role of SRSF1 in regulating incisor progenitors that are required for continual tissue renewal, we next focused on studying the function of SRSF1 and understanding its progenitor-specific regulatory role.

SRSF1 regulates alternative splicing events related to maintaining the survival and proliferation of dental progenitors

To detect alternative splicing events governed by the main splicing regulator SRSF1, we performed bulk RNA-seq of dissected adult dental epithelium from 3 control and 4 $K14^{CreER};Srsf1^{fl/fl}$ mutant mice. Using the JuncBASE (junction based analysis of splicing events) tool (Brooks et al., 2011), we evaluated and classified alternative splicing events with a false discovery rate lower than 0.1. We identified 170 alternative splicing events strongly associated with *Srsf1* deletion with the absolute “percent spliced in” value (Δ PSI) higher than 10% (Figure 2A; Table S1). Almost half of these SRSF1-regulated alternative splicing events corresponded to cassette exons (CA-exons), also known as exon skipping (Figure 2A). The pervasive effect of *Srsf1* deletion on CA-exon splicing was further supported by a skew toward p values that were lower than expected (Figure 2B). A larger proportion of the CA-exon events identified had Δ PSI lower than -10% , indicating that *Srsf1* mutation was more associated with the skipping of exons rather than inclusion (Figure 2C). All 170 alternative splicing events were plotted in a heatmap (Figure 2D), revealing a trend toward a higher exon inclusion rate in control samples or, in other words, more exon skipping events in $K14^{CreER};Srsf1^{fl/fl}$ mutants. Together, these data indicate that CA-exon events were highly prevalent with the deletion of *Srsf1*.

To identify direct binding targets of SRSF1, we compared published cross-linking immunoprecipitation (CLIP) tags (Sanford et al., 2008; Pandit et al., 2013; Anczuków et al., 2015) with the bulk RNA-seq alternative spliced gene list (Table S1). Therefore, 52 overlapping targets were found as putative alternatively spliced binding targets of SRSF1 (Table S2). To predict the bio-

logical impact of alternatively spliced targets upon *Srsf1* deletion, we analyzed the topological correlation between alternatively spliced SRSF1 binding targets (Table S2) and differentially expressed genes in *Srsf1* mutants (Table S3) using the STRING plot (Figure S4A). Ten highlighted putative SRSF1 targets were identified, grouping into different clusters (Figure S4A). The rankings of $|\Delta$ PSI| of these highlighted targets are shown in the heatmap (Figure 2D).

Next, we assessed the accuracy of splicing changes from the RNA-seq data. Then, we quantitatively visualized sequencing reads aligned to gene annotations in control and *Srsf1* mutants with Sashimi plots (Figure 3). To further validate the PSI of 10 SRSF1 binding targets, we performed reverse-transcriptase PCR (RT-PCR) in triplicate, using primers flanking the shaded CA-exons to amplify both isoforms that included and excluded the exon (Figure 3). All 10 targets showed significant downregulation of their full-length transcripts and upregulation of their truncated transcripts upon *Srsf1* deletion (Figure 3), consistent with the quantification of the Sashimi plots (Figures S5A–S5J).

To determine the biological functions altered by *Srsf1* deletion, the STRING analysis was cross-referenced with Gene Ontology (GO) clusters. GO analysis was performed on the list of SRSF1 translational genes (Table S3) using the DAVID database for functional annotation under the category of “Biological Process.” Genes clustered into two main terms: (1) cell death and DNA damage or (2) cell cycling (Figure S4B). These assignments were consistent with our observation that cell death was increased and proliferation was reduced following *Srsf1* deletion. The biological functions of targets located within the main branch in the STRING plot (Figure S4A, blue-labeled targets), namely *Cdc45*, *Incenp*, *Rif1*, and *Ncor1*, were closely related to cell survival and cycling, as indicated in the GO clusters. In contrast, the yellow-labeled SRSF1 targets, which were reported as genes functioning during cell adhesion and RNA splicing, were not directly associated with the two main biological GO clusters. In addition, they were located outside of the main topological branch in the STRING plot (Figure S4A), suggesting that they are less likely to be responsible for gene expression or histological changes after *Srsf1* deletion. Because we observed significant changes in cell proliferation and survival upon *Srsf1* deletion, we proceeded to analyze the roles of *Cdc45*, *Incenp*, *Rif1*, and *Ncor1* in maintaining dental tissue homeostasis and supporting tissue renewal.

To address how the ubiquitously expressed SRSF1 protein can regulate distinct functions in specific cell types, we analyzed the expression of its 4 putative binding targets related to cell survival and cycling in the adult laCL. All 4 targets were expressed at significantly higher levels in the proliferating IEE (Figures 4A–4H) compared with the other regions of the dental epithelium. Among them, CDC45 and INCENP were most strongly enriched in the IEE (Figures 4A–4B', 4E, and 4F), whereas RIF1 and NCOR1 were mainly expressed in the IEE and in the laCL (Figures 4C–D', 4G, and 4H). Since we observed low levels of background staining using the INCENP, RIF1, and NCOR1 antibodies (Figures 4B–4D'), we also examined their expression in a published single cell RNA-seq dataset (Sharir et al., 2019) (Figures S5K–S5O) and using *in situ* hybridization (Figures S6A–S6C). Together, our findings suggest that the progenitor-specific phenotype of SRSF1 arises because it controls alternative splicing of progenitor-enriched targets.

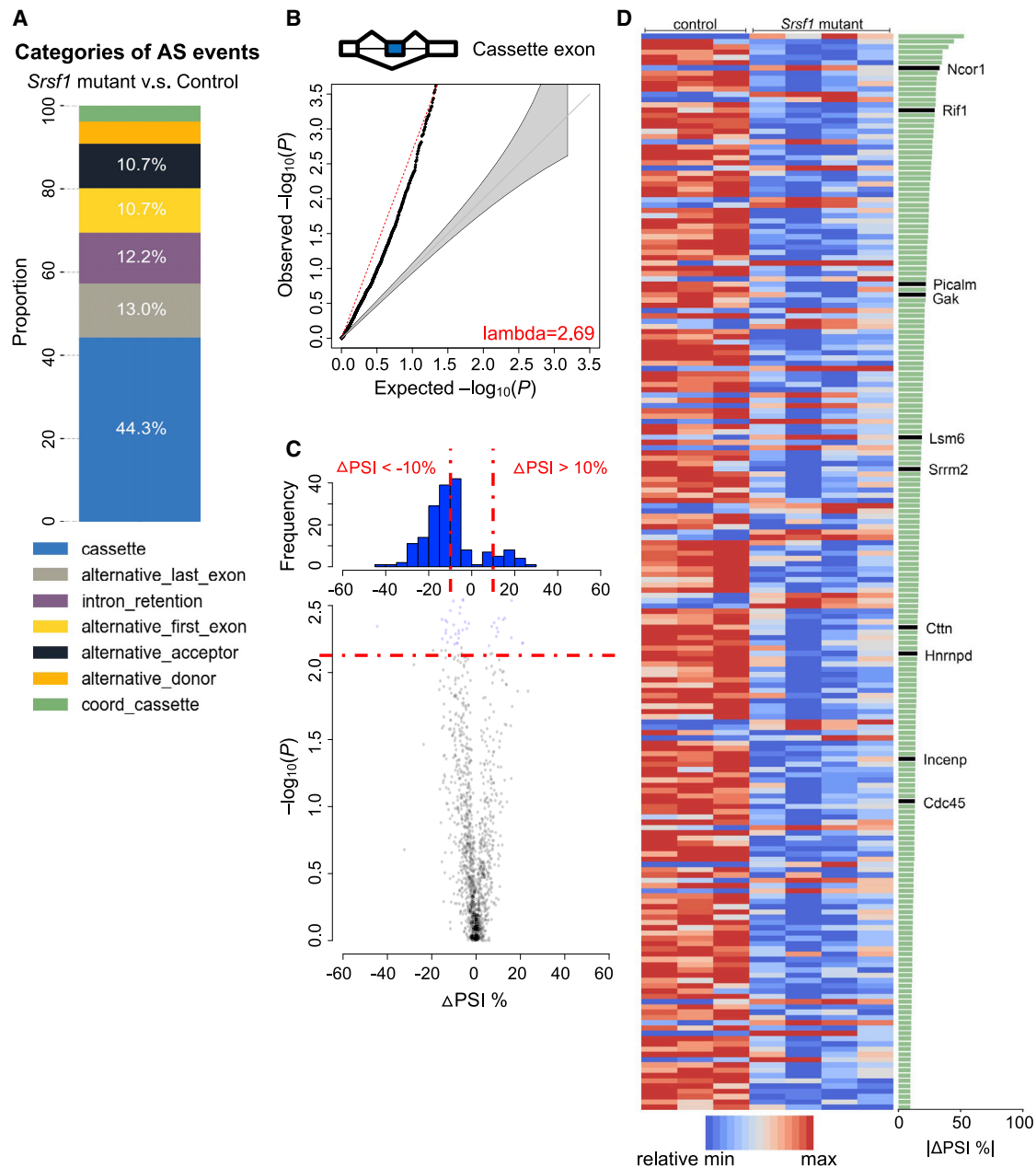


Figure 2. SRSF1 governs a large number of alternative splicing events in the adult mouse laCL

(A) Categories of alternative splicing events significantly associated with *Srsf1* deletion versus control adult mouse laCL from bulk RNA-seq.

(B) Q-Q plot analysis of cassette exon (CA-exon) splicing events.

(C) Volcano plot analysis of alternative splicing events upon deletion of *Srsf1*. Red dashed/dotted lines indicate a large magnitude of splicing change percent spliced in $|\Delta\text{PSI}| \geq 10\%$ (top) or a significant p value (bottom).

(D) Heatmap of upregulated and downregulated alternative splicing events between the control and *K14^{CreER};Srsf1^{fl/fl}* (*Srsf1* mutant) laCL. The genes that contain splicing events that are highly likely to be directly regulated by SRSF1 are labeled and highlighted in black. Red or blue color indicates upregulation or downregulation of each splicing event, respectively. See also Figure S4.

SRSF1 plays an essential role in maintaining progenitors but is dispensable in differentiated cells in the adult mouse small intestine

Our data suggest that SRSF1 plays a specific role in splicing key targets required for dental progenitor function. Given that *in vivo* studies have shown that SRSF1 is required to maintain normal

development of various organs at different stages (Xu et al., 2005; Kanadia et al., 2008; Katsuyama et al., 2019), we therefore considered whether the regulation of progenitor function by SRSF1 was conserved across different tissues. To address this question, we tested whether SRSF1 serves a similar progenitor-specific function in another highly regenerative epithelium,

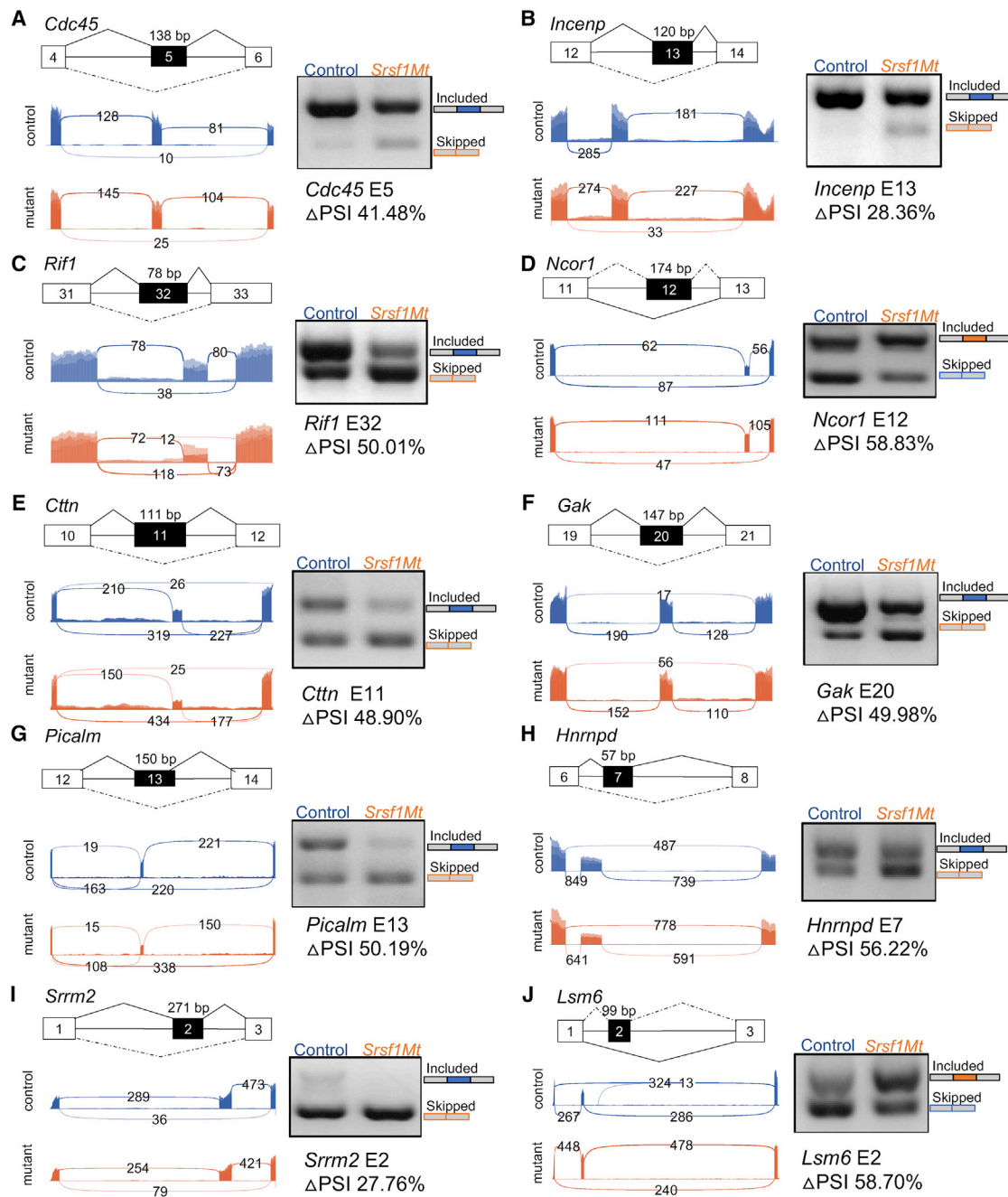


Figure 3. Deletion of *Srsf1* alters alternative splicing of its binding targets

(A–J) SRSF1-regulated CA-exons events of *Cdc45* (A), *Incenp* (B), *Rif1* (C), *Ncor1* (D), *Ctnn* (E), *Gak* (F), *Picalm* (G), *Hnrnpd* (H), *Srrm2* (I), and *Lsm6* (J) in the mouse incisor laCL. For each gene, exons and introns are indicated in scaled diagrams. CA-exons are shaded. Included exon transcripts are spliced with solid lines, and skipped transcripts are spliced with dashed lines. The exon number and the size of CA-exons are labeled in and on top of the diagram, respectively. Sashimi plots (below the scaled diagrams) were used to quantitatively visualize splice junctions in control and *Srsf1* mutants (*Srsf1* Mt). Sashimi plots are depicted under the gene structure, with each peak representing read coverage of each exon. RT-PCR validation of each gene is shown at the right side of the panel, with representative gel images and quantification of the Δ PSI expression in *Srsf1* mutants. The representative cropped gel images are shown from 3 biological replicates. All quantitative data are shown as mean \pm SD (* p < 0.05 and ** p < 0.001). See also Figure S5.

the adult mouse small intestine. In the intestinal crypts, lysozyme-secreting differentiated Paneth cells are intermingled between *Lgr5*⁺ intestinal stem cells, which divide daily to give rise to transit-amplifying (T-A) progenitors (Barker et al., 2007). T-A

cells proliferate and contribute to various secretory and absorptive cell lineages in the villi (reviewed in Zwick et al., 2019). To determine whether SRSF1 also has a distinct cellular function in different intestinal cell types, we deleted *Srsf1* in the adult

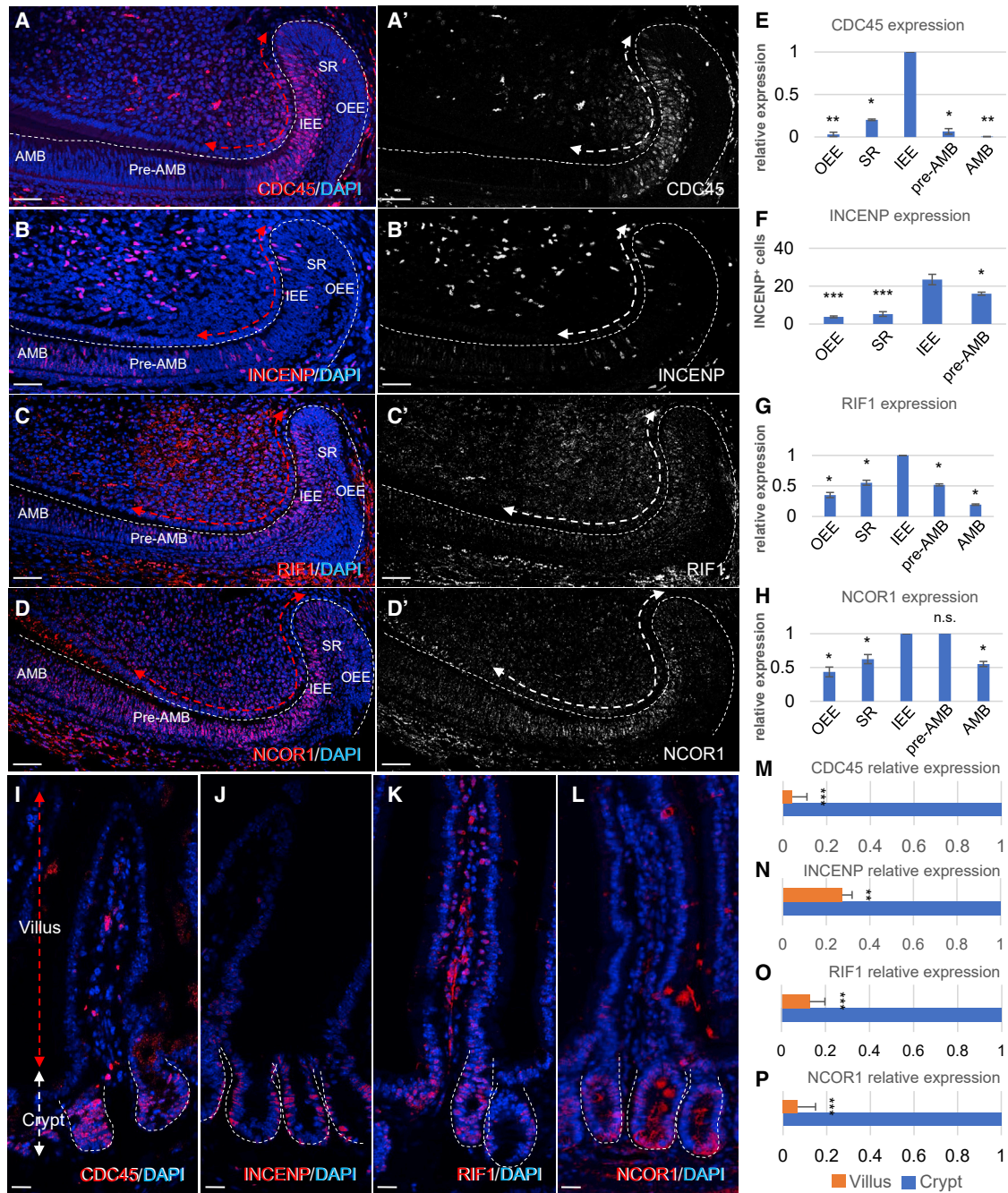


Figure 4. SRSF1 binding targets are highly expressed in proliferating IEE and crypts in the laCL and the small intestine, respectively

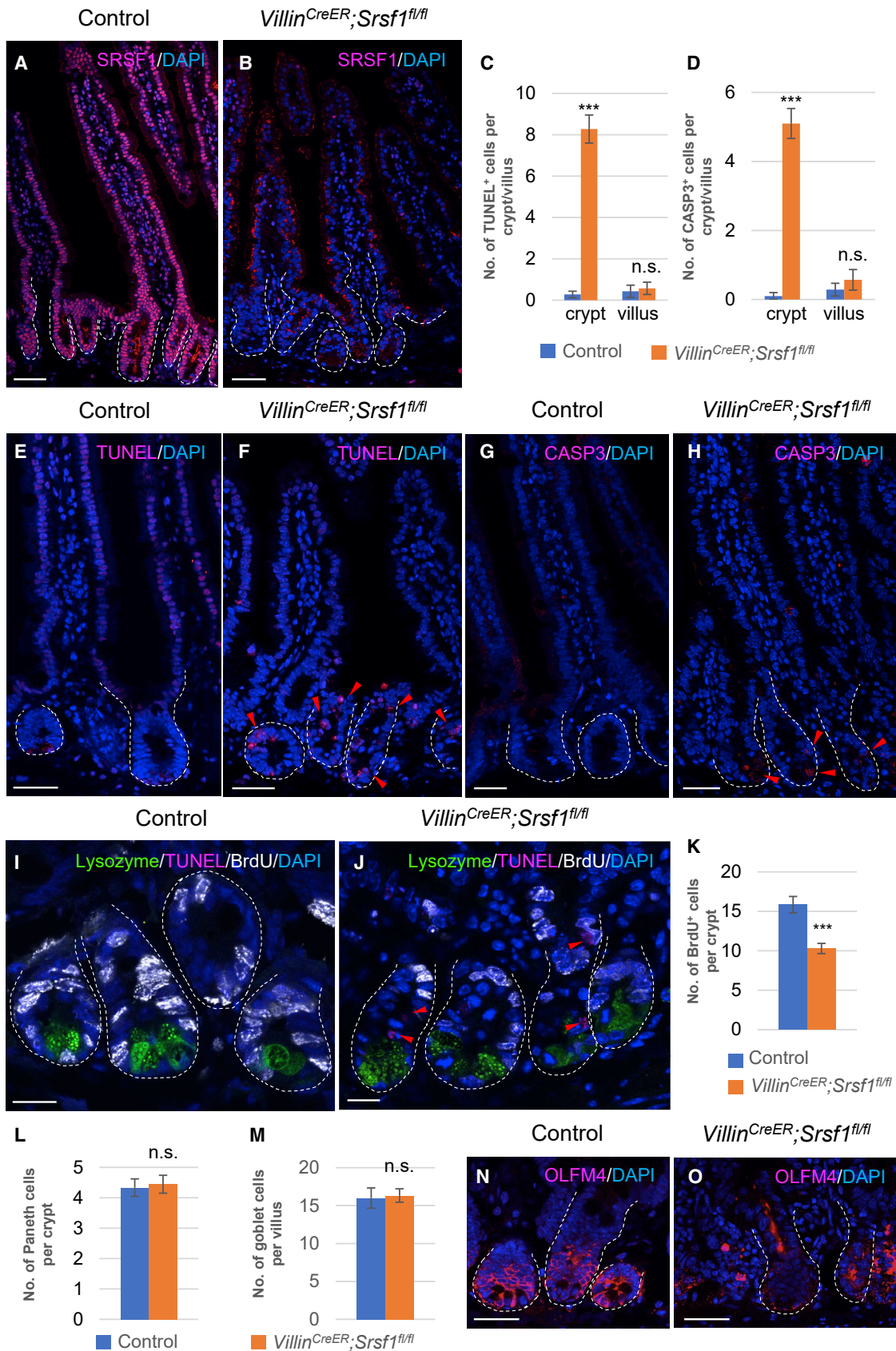
(A–D) Immunostaining of CDC45 (A), INCENP (B), RIF1 (C), and NCOR1 (D) in the laCL. Red dashed lines with arrowheads mark higher expression regions of the proteins. INCENP antibody staining showed strong background in ameloblasts, making it hard to quantify in AMB region.

(A'–D') Grayscale images of protein expression of CDC45 (A'), INCENP (B'), RIF1 (C'), and NCOR1 (D') in the laCL. White dashed lines with arrowheads mark higher expression regions of the proteins.

(E–H) Quantification of regional protein expression of CDC45 (E), INCENP (F), RIF1 (G), and NCOR1 (H). OEE, outer enamel epithelium; SR, stellate reticulum; IEE, inner enamel epithelium; pre-AMB, pre-ameloblast; AMB, ameloblast. Dashed lines outline laCL. Images were stitched manually, selecting a common feature appearing in the overlapping region.

(I–L) Immunostaining of CDC45 (I), INCENP (J), RIF1 (K), and NCOR1 (L) in the small intestine. Red dashed lines with arrowheads mark the villus region. White dashed lines with arrowheads mark the crypt region. Dashed lines outline small intestine crypts. INCENP antibody showed strong background; therefore, *in situ* hybridization data were added in Figures S6A and S6A'.

(M–P) Quantification of regional protein expression of CDC45 (M), INCENP (N), RIF1 (O), and NCOR1 (P). Representative images and quantitative data are shown. All quantitative data are shown as mean \pm SD (* $p < 0.05$, ** $p < 0.001$, *** $p < 0.001$, and n.s. represents not significant). Scale bar represents 50 μ m in (A–D') and 20 μ m in (I–L). See also Figure S6.



(legend on next page)

mouse small intestine by crossing an *Srsf1* conditional allele (*Srsf1^{fl/fl}*) (Xu et al., 2005) with the pan-intestinal epithelial *VillinCre^{ER}* (El Marjou et al., 2004).

As in the adult mouse incisor epithelium, SRSF1 was also expressed ubiquitously in the small intestinal epithelium throughout the crypt-villus axis, suggesting a potential role in intestinal epithelial cell dynamics (Figure 5A). Three days after two consecutive tamoxifen injections, SRSF1 expression was reduced significantly in the epithelium of both crypts and villi (Figure 5B). As determined by both TUNEL assay (Figures 5C and 5F) and cleaved caspase 3 (CASP3) immunostaining (Figures 5D and 5H), increased cell death was observed specifically in the intestinal crypts upon *Srsf1* deletion compared with the controls (Figures 5E and 5G). TUNEL⁺ cells were found among the BrdU⁺ progenitor-enriched region in the intestinal crypts in *VillinCre^{ER};Srsf1^{fl/fl}* mutants, without overlapping with the Paneth cells at the crypt base (Figures 5I and 5J). Correspondingly, the number of BrdU⁺ cells was reduced (Figures 5I–5K). Neither mature Paneth cells in the crypt (Figures 5I, 5J, and 5L) nor the number of differentiated goblet cells in the villi (Figure 5M) was obviously affected by the loss of SRSF1. Taken together, our results demonstrate that SRSF1 plays a critical role in maintaining the cycling population of T-A cells in intestinal crypts of adult mice, whereas it is not required for the survival of differentiated cells in either crypts or villi. These data indicate a similar progenitor-specific function of SRSF1 in another epithelial tissue distinct from the adult mouse incisor. Interestingly, the expression of the intestinal stem cell marker, OLFM4, was also decreased in the *VillinCre^{ER};Srsf1^{fl/fl}* compared with the control (Figures 5O and 5N), suggesting that there might be feedback from progenitors to stem cells in the adult mouse intestinal epithelium.

To determine whether these same alternatively spliced putative binding targets of SRSF1 can be identified in the intestinal epithelium, we used fluorescence-activated cell sorting (FACS) to purify crypt cells and performed RT-PCR for validation. Similar changes in splicing events of all 4 genes were observed in *VillinCre^{ER};Srsf1^{fl/fl}* mutants, showing a significant downregulation of their full-length transcripts and upregulation of their truncated transcripts upon *Srsf1* deletion (Figures S6D and S6E). In addition, we also analyzed the expression of these 4 putative binding targets in the intestinal epithelium. CDC45, INCENP, RIF1, and NCOR1 were all expressed at significantly higher levels in crypt cells (Figures 4I–4P) compared with villus cells, providing another piece of evidence in a different epithelial

system to support the hypothesis that the progenitor-specific phenotype of SRSF1 arises because it controls alternative splicing of progenitor-enriched targets.

Srsf1 mutation activates the p53/p21 pathway, impairing cellular function of both dental and intestinal progenitors

The functions of all 4 SRSF1 binding targets have been linked to the p53/p21 pathway via various *in vitro* studies (Battaglia et al., 2010; Datta et al., 2017; Sun et al., 2019; Eke et al., 2020). Given that defects in cell proliferation and cell survival were two main consequences of *Srsf1* deletion in the adult mouse laCL and small intestine and changes in the p53 pathway are key to both cell cycling and apoptosis (reviewed in Bartek and Lukas, 2001; reviewed in Harris and Levine, 2005), we hypothesized that SRSF1 might control the activity of P53 and P21 through the regulation of the splice variants of *Cdc45*, *Incenp*, *Rif1*, and *Ncor1*. Therefore, we next analyzed the expression of P53 and P21 in the *K14^{CreER};Srsf1^{fl/fl}* and *Villin^{CreER};Srsf1^{fl/fl}* mutants.

In both adult mouse laCL and small intestine crypts, P53 was not detectable in the controls (Figures 6A, 6A', and 6F), whereas its immunostaining signal was upregulated in IEE progenitors in *K14^{CreER};Srsf1^{fl/fl}* mutants (Figures 6B, 6B', and 6E) and in the intestinal crypt progenitors in *Villin^{CreER};Srsf1^{fl/fl}* mutants (Figures 6G and 6J). The immunostaining of the p53-dependent cell cycle regulator P21 was also increased in the similar IEE region in laCLs (Figures 6C–6E), as well as in the intestinal crypts (Figures 6H–6J) upon *Srsf1* deletion. Together, these data suggest that misregulation of alternative splicing events due to loss of SRSF1 activates P53 to stabilize P21, which then inhibits the activity of cyclin-dependent kinase to arrest cell cycle progression. In turn, inappropriate activation of the p53/p21 pathway stimulates apoptosis.

AMO-mediated exon exclusion of targeted genes recapitulates loss of Srsf1

Although traditionally considered as a splicing regulator, SRSF1 has been shown to regulate other cellular functions outside of alternative splicing (Das and Krainer, 2014). To understand whether the observed activation of p53/p21 is due to mis-splicing of the identified targets or other SRSF1-dependent functions, we reasoned that inducing the specific mis-splicing events without affecting *Srsf1* levels could help identify how SRSF1 is acting. We tested this approach using antisense morpholino oligonucleotides

Figure 5. SRSF1 is required for maintaining the survival of intestinal progenitors, while it is dispensable for the differentiated cell populations (A and B) Immunostaining of SRSF1 in control (A) and *Villin^{CreER};Srsf1^{fl/fl}* (B) in the mouse small intestine. Significantly reduced expression of SRSF1 upon intestinal epithelial deletion of *Srsf1* (B). Images were stitched manually, selecting a common feature appearing in the overlapping region. (C and D) Quantification of the number of TUNEL⁺ cells (C) and CASP3⁺ cells (D) in the crypts and villi, respectively. (E–H) Detection of apoptosis using TUNEL assay (E and F) and immunostaining of CASP3 (G and H) in control (E and G) and *Villin^{CreER};Srsf1^{fl/fl}* (F and H) small intestine. Increased apoptotic cells (red arrowheads) can be detected in *Srsf1* mutants (F and H). (I and J) Triple-labeling—TUNEL (red) with immunostaining of Paneth cell marker, lysozyme (green) and BrdU (gray) in control (I) and *Villin^{CreER};Srsf1^{fl/fl}* (J) in adult mouse small intestine. Increased cell death (red arrowheads) was detected specifically in the proliferating region enriched in BrdU⁺ (gray) cells (J). The number of Paneth cells (green) shows no difference upon *Srsf1* deletion in the small intestine (J), compared with control (I). (K–M) Number of BrdU⁺ cells (K), Paneth cells (L) in the crypt, and goblet cells (M) per crypt-villus unit in control and *Villin^{CreER};Srsf1^{fl/fl}* small intestine. All quantitative data are shown as mean ± SD (*** p < 0.001 and n.s. not significant). (N and O) Immunostaining of OLFM4 in control (N) and *Villin^{CreER};Srsf1^{fl/fl}* (O) in the mouse small intestine. Significantly reduced expression of OLFM4 upon *Srsf1* deletion (O). Dashed lines outline small intestine crypts. Representative images and quantitative data are shown. Scale bar represents 50 μm in (A) and (B), (E–H), (N), and (O) and 20 μm in (I) and (J).

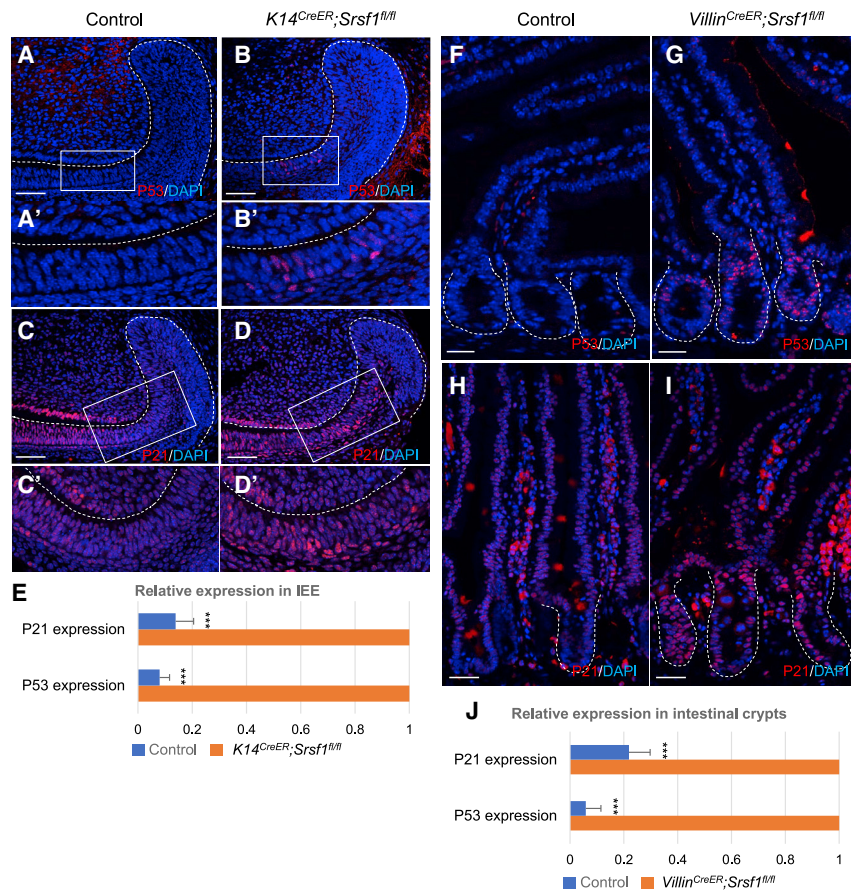


Figure 6. Deletion of *Srsf1* activates p53/p21 pathway, leading to impaired function of both dental and intestinal progenitors

(A–B') Immunostaining of P53 in the control (A) and *K14^{CreER};Srsf1^{fl/fl}* (B) laCL. Enlarged images of boxed regions are displayed in (A') and (B'), respectively.

(C–D') Immunostaining of P21 in the control (C) and *K14^{CreER};Srsf1^{fl/fl}* (D) laCL. Enlarged images of boxed regions are displayed in (C') and (D'), respectively.

(E) Quantification of regional P21 and P53 expression in the IEE.

(F and G) Immunostaining of P53 in the control (F) and *Villin^{CreER};Srsf1^{fl/fl}* (G) small intestine.

(H and I) Immunostaining of P21 in the control (H) and *Villin^{CreER};Srsf1^{fl/fl}* (I) small intestine.

(J) Quantification of regional P21 and P53 expression in the small intestine. Dashed lines outline laCL and small intestine crypts. Representative images and quantitative data are shown. All quantitative data are shown as mean ± SD (***) $p < 0.001$. Scale bar, 50 μ m.

(AMOs), which are splice-switching molecules that bind to a reverse complementary sequence of a pre-mRNA target. Steric blocking of SRSF1's ability to bind and promote exon inclusion results in an exon skipping event. This allows for the following possible splice site to be used, thus mimicking the exon skipping event observed in the *Srsf1* mutant (Figure 7A). Primary dental epithelial cells harvested from the progenitor-rich cervical loop region (Chavez et al., 2014) and primary intestinal cells harvested from organoid crypts (Thorne et al., 2018) were cultured and transfected with a control AMO or an AMO targeting *Cdc45* exon (E)5, *Incenp* E13, or *Rif1* E32 for 48 h. Each target-specific AMO induced the respective exon skipping event observed *in vivo* without affecting the levels of *Srsf1*, as observed by RT-PCR (Figures 7B and 7F). Furthermore, immunostaining showed increased activation of both P53 and P21 with the target-specific AMO for both primary dental epithelial cells or intestinal epithelial cells (Figures 7C–7E and 7G–7I). These data indicate that a major role of SRSF1 in the incisor is as a splicing regulator of these target genes, which are essential for the survival of highly proliferative progenitor cells.

DISCUSSION

To maintain tissue homeostasis and regenerative capability, proliferative progenitors must generate various cell populations. Among the mechanisms contributing to the regulation of self-renewal, proliferation, and differentiation of progenitor cells,

alternative splicing can play a significant role in producing the complex repertoire of protein isoforms required from embryonic stages to adulthood, as well as under health and disease conditions. In this study, using the adult mouse incisor and small intestine as two fast-cycling *in vivo* model systems, we identified a mechanism by which the ubiquitously expressed

SRSF1 splicing factor governs alternative splicing in a progenitor-specific manner. Loss of SRSF1 function resulted in the misregulation of alternative splicing events, thus activating p53/p21 signaling and leading to cell cycle arrest and apoptosis of progenitors. Together, our findings reveal an intricate alternative splicing regulatory system in rapidly renewing tissues.

Progenitor-specific alternative splicing regulation

Previously reported progenitor-specific function of splicing regulators mainly focused on identifying pro-pluripotent splicing events using pre-enriched human/mouse embryonic stem cells or mouse neural stem cells (Atlasi et al., 2008; Hayakawa-Yano et al., 2017). However, many splicing regulators exhibit broad expression patterns (Kalsotra et al., 2008; Yeo et al., 2009; Damianov and Black, 2010), pointing to a need to look beyond stem cells to reveal distinct cellular functions of splicing regulators at the tissue or organ level. In this study, by interrogating cells at various stages of differentiation, our findings identified a key role of SRSF1 in specifically maintaining progenitor proliferation and survival during homeostatic turnover in adult epithelial tissues. Interestingly, instead of having a regionally restricted expression pattern, the master splicing regulator SRSF1 was expressed ubiquitously and yet found to specifically govern the splicing of genes enriched in the progenitors in the adult mouse laCL. Even though SRSF1 was also expressed in other more differentiated cell types, it was dispensable for their function and survival. To rule out the possibility that the dental

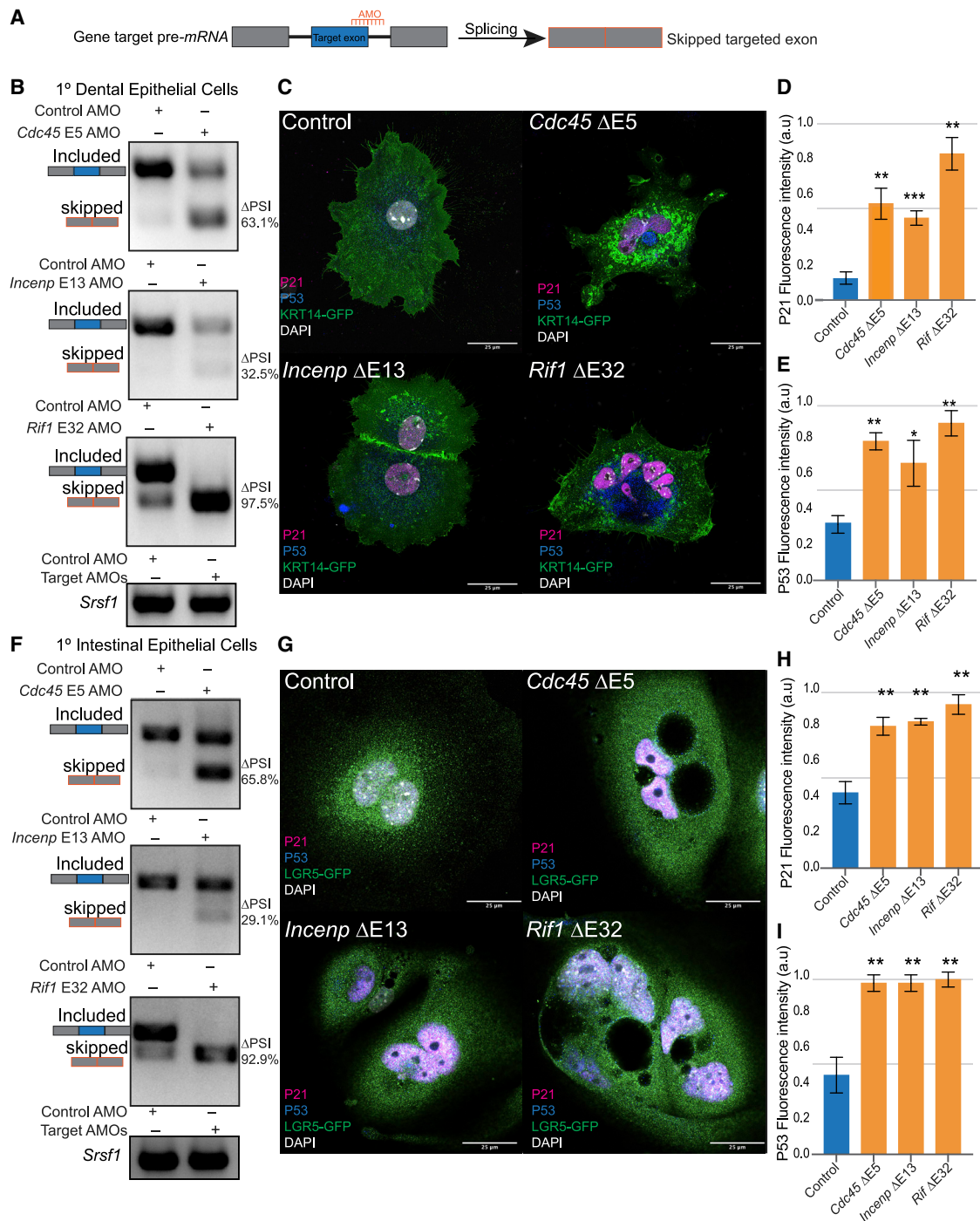


Figure 7. AMO-mediated exon exclusion of targeted genes recapitulates loss of *Srsf1* phenotype

(A) Schematic of AMO-mediated exon skipping event.

(B) Representative RT-PCR of control and target gene AMO transfections in primary dental epithelial cells and resulting Δ PSI upon transfection.

(C) Representative immunocytochemistry staining for P21 (magenta) and P53 (blue) in control AMO and individual target gene AMOs-treated primary dental epithelial cells as marked by KRT14-mGFP (green). Δ E denotes the exon skipped upon AMO transfection.

(D and E) Quantification of regional P21 and P53 expression, respectively, in primary dental epithelial cells.

(F) Representative RT-PCR of control AMO and target gene AMO transfections in primary intestinal epithelial cells and resulting Δ PSI upon transfection.

(G) Representative immunocytochemistry staining for P21 (magenta) and P53 (blue) in control AMO and individual target gene AMOs-treated primary intestinal epithelial cells as marked by LGR5-mGFP (green). Δ E denotes the exon skipped upon AMO transfection.

(H and I) Quantification of regional P21 and P53 expression, respectively, in primary intestinal epithelial cells. All quantitative data are shown as mean \pm SD (***) $p < 0.001$). Scale bar, 25 μ m.

progenitor-specific defects observed in *K14^{CreER};Srsf1^{fl/fl}* mutant laCL were indirectly introduced from potential disruption in other cell types in which *K14^{CreER}* was activated, we further included *Shh^{CreER};Srsf1^{fl/fl}* to allow more restricted deletion of *Srsf1* in lower IEE in the incisor cervical loops (Seidel et al., 2010) (Figure S7). In this knockout system, we observed similar disrupted function specifically in dental progenitors (Figures S7E–S7L), as well as similar changes in alternative splicing of 4 SRSF1 targets (Figure S7M). These data support the notion that the splicing defects were caused by a specific impact on dental progenitors upon *Srsf1* deletion.

In adult organs that require rapid cell turnover to counterbalance constant tissue loss, stem cells and progenitors play an essential role in ensuring these systems' normal function. In recent years, numerous studies have identified cell plasticity in committed cell types. When high levels of cell death occur in the progenitor pool upon acute tissue injury, differentiated cells can undergo dedifferentiation or transdifferentiation to replenish the loss in the progenitor niche to repair the tissue (reviewed in Varga and Greten, 2017; reviewed in McKinley et al., 2020). For example, in the small intestine, cellular plasticity has been observed in numerous immature and committed cell types, which can dedifferentiate to restore intestinal homeostasis upon ablation of *Lgr5+* intestinal stem cells (Jadhav et al., 2017; Yan et al., 2017). Therefore, maintaining ubiquitous expression of SRSF1 might be essential for the dedifferentiation or transdifferentiation of cells to quickly restore progenitor cells and support tissue injury repair.

In vivo analysis of the cellular mechanism of alternative splicing regulation during adult tissue homeostasis and renewal

Studies performed in human or mouse embryonic stem cells, as well as in cancer cells, have provided important information about how alternative splicing events change in response to different stages or under disease conditions (Salomonis et al., 2010; Xu et al., 2018; reviewed in Qi et al., 2020). However, whether all *in vitro* data are representative or able to recapitulate *in vivo* conditions remains debatable. For example, cross-regulation and antagonism between SRSF1 and SRSF3 have been reported through *in vitro* studies (Jumaa and Nielsen, 1997; Gonçalves et al., 2009; Sun et al., 2010). In this study, we did not observe a strong inter-regulatory function between these two SR proteins in the adult mouse laCL. Although 60% of alternative splicing events regulated by SRSF3 corresponded to CA-exons (Figure S3L), similar to SRSF1 (Figure 2A), only three overlapping genes were governed by SRSF1 and SRSF3, and no antagonistic regulation was identified (data not shown). A slight downregulation of RNA expression of *Srsf3* was detected in the *K14^{CreER};Srsf1^{fl/fl}* mutant laCL (Figure S3M). However, due to cell heterogeneity in the dental tissue, no solid conclusion can be drawn regarding whether *Srsf1* and *Srsf3* can compensate for each other in distinct cell types. Compared with the relatively simpler *in vitro* culture systems that have one or a small number of cell types, single-cell RNA-seq will be needed to answer this question in the incisor laCL. It will be important to consider tissue-specific differences or potential variations between *in vitro* and *in vivo* studies in future work.

Furthermore, cellular responses were observed *in vivo* upon *Srsf1* deletion in laCLs that could not be detected through *in vitro* analysis. Consistent with mGFP expression reporting Cre-mediated recombination throughout the *K14^{CreER};Srsf1^{fl/fl}* mutant laCL, the expression of SRSF1 in IEE cells, SI cells, pre-ameloblasts, and ameloblasts was almost undetectable 1 to 2 days after tamoxifen injection (1–2 days post induction [dpi]), whereas SRSF1 was still highly expressed in cells in the stellate reticulum and OEE regions (Figures S2B–B'', S2F, and S2G). SRSF1 expression started to decrease in the stellate reticulum and OEE at 3 dpi, and the reduction became evident at 4 dpi (Figures S2H and S2I). Recovery of SRSF1 expression in the IEE initiated at around 4 dpi (Figure S2I). By 5 dpi, a more pronounced expression of SRSF1 was observed in the IEE (Figure S2J). These data together suggest that the perdurance of SRSF1 varies in different cell types in the adult mouse laCL, which could inform further understanding of the cellular regulation of alternative splicing during injury repair.

Together, our findings define a mechanism by which SRSF1-dependent alternative splicing events regulate homeostasis in adult tissues, revealing a paradigm for cell-type-specific splicing factor function. We identified a conserved mechanism of SRSF1 function in both the incisor and small intestine, suggesting a fundamental role of this splicing factor during development and posing new questions for future research into the regulation of alternative splicing in tissue regeneration and injury repair.

Limitations of the study

A major limitation of conducting *in vivo* analysis on alternative splicing regulation is the difficulty in obtaining sufficient protein. For example, more than 250 mice (500 laCLs) of relatively similar age would be needed to obtain enough SRSF1 protein to perform RNA immunoprecipitation, such as CLIP. Therefore, we cross-referenced to published CLIP data from *in vitro* culture of HEK293T cells, mouse embryo fibroblasts, MCF-10A cells, and HeLa cells (Sanford et al., 2008; Pandit et al., 2013; Anczuków et al., 2015). Next, the alternatively spliced transcripts of all 10 putative binding targets (Table S2) were validated through RT-PCR, strongly suggesting that they were directly regulated by SRSF1. Thus, immediate splicing responses were recorded 1 day after tamoxifen injection. Using AMOs, we validated the effects of the particular exon exclusion for *Cdc45*, *Incepn*, and *Rif1* in the activation of p53/p21. However, inducing an exon inclusion event as seen in *Ncor1* is much more challenging, given the frequency of sequences involved in splicing found within the large intronic regions. Nevertheless, the robust activation of P53 and P21 upon the exon skipping events in *Cdc45*, *Incepn*, and *Rif1* gives us confidence to suggest important roles for these targets in the proper maintenance of adult epithelial progenitors.

STAR★METHODS

Detailed methods are provided in the online version of this paper and include the following:

- KEY RESOURCES TABLE
- RESOURCE AVAILABILITY
 - Lead Contact and Materials Availability
 - Data and Code Availability

- EXPERIMENTAL MODELS AND SUBJECT DETAILS
 - Animals
- METHOD DETAILS
 - Tamoxifen injection
 - BrdU injection
 - Tissue preparation
 - Immunofluorescence assays
 - TUNEL assay
 - Hematoxylin & Eosin (H&E) staining
 - Bulk RNA-Seq and analysis
 - Bulk RNA-Seq alternative splicing analysis
 - Reverse transcription PCR (RT-PCR)
- QUANTIFICATION AND STATISTICAL ANALYSIS
 - Statistical analysis
 - ImageJ image analysis

SUPPLEMENTAL INFORMATION

Supplemental information can be found online at <https://doi.org/10.1016/j.devcel.2022.01.011>.

ACKNOWLEDGMENTS

We thank A. Rathnayake, B. Hoehn, E. Sandoval, and S. Alto for technical assistance, Drs. J. Hu, K. McKinley, P. Marangoni, R. Zwick, T. Huycke, and A. Sharir, members of the Klein, Floor, Brooks, and Goodwin labs for helpful discussions, Dr. K. Seidel for importing and maintaining the *Srsf1^{fl/fl}* and *Srsf3^{fl/fl}* mouse lines at the beginning of the project, and the UCSF Functional Genomics Core for help with RNA-seq. This work was funded by NIDCR R01-DE024988 and R35-DE026602 to O.D.K. H.S.J. was supported by National Research Foundation of Korea (NRF) 2016R1A5A2008630.

AUTHOR CONTRIBUTIONS

Conceptualization, T.Y., O.C., and O.D.K.; methodology, T.Y., O.C., and O.D.K.; investigation, T.Y., O.C., H.-Y.K., A.D.T., and T.W.; writing—original draft, T.Y. and O.D.K.; writing, review, and editing, T.Y., O.C., H.-Y.K., A.D.T., T.W., Q.L., M.H.B.-H., S.N.F., H.-S.J., A.N.B., and O.D.K.; funding acquisition, O.D.K.; supervision, O.D.K.

DECLARATION OF INTERESTS

The authors declare no competing interests.

INCLUSION AND DIVERSITY

The sex balance of our samples was included as part of our experimental designs. Our laboratories take pride in fostering a diverse and inclusive environment, and we strive to make equitable opportunities for all our trainees. The authors of this paper identify as members of one or more of the following communities: AAPI, Black, Differently Able, Latinx, and LGBTQ+. Also, in this study, one or more of the authors received support from a program designed to increase minority representation.

Received: April 27, 2020

Revised: November 4, 2021

Accepted: January 18, 2022

Published: February 23, 2022

REFERENCES

Anczuków, O., Akerman, M., Cléry, A., Wu, J., Shen, C., Shirole, N.H., Raimer, A., Sun, S., Jensen, M.A., Hua, Y., and Allain, F.H.T. (2015). SRSF1-regulated alternative splicing in breast cancer. *Mol. Cell* **60**, 105–117.

Atlati, Y., Mowla, S.J., Ziaee, S.A., Gokhale, P.J., and Andrews, P.W. (2008). OCT4 spliced variants are differentially expressed in human pluripotent and nonpluripotent cells. *Stem Cells* **26**, 3068–3074.

Barker, N., Van Es, J.H., Kuipers, J., Kujala, P., Van Den Born, M., Cozijnsen, M., Haegebarth, A., Korving, J., Begthel, H., Peters, P.J., and Clevers, H. (2007). Identification of stem cells in small intestine and colon by marker gene *Lgr5*. *Nature* **449**, 1003–1007.

Bartek, J., and Lukas, J. (2001). Mammalian G1- and S-phase checkpoints in response to DNA damage. *Curr. Opin. Cell Biol.* **13**, 738–747.

Battaglia, S., Maguire, O., Thorne, J.L., Hornung, L.B., Doig, C.L., Liu, S., Sucheston, L.E., Bianchi, A., Khanim, F.L., Gommersall, L.M., and Coulter, H.S. (2010). Elevated NCOR1 disrupts PPAR α/γ signaling in prostate cancer and forms a targetable epigenetic lesion. *Carcinogenesis* **31**, 1650–1660.

Brooks, A.N., Yang, L., Duff, M.O., Hansen, K.D., Park, J.W., Dudoit, S., Brenner, S.E., and Graveley, B.R. (2011). Conservation of an RNA regulatory map between *Drosophila* and mammals. *Genome Res.* **21**, 193–202.

Chavez, M.G., Hu, J., Seidel, K., Li, C., Jheon, A., Naveau, A., Horst, O., and Klein, O.D. (2014). Isolation and culture of dental epithelial stem cells from the adult mouse incisor. *J. Vis. Exp. (Jove)* **87**, e51266.

Cheng, Y., Luo, C., Wu, W., Xie, Z., Fu, X., and Feng, Y. (2016). Liver-specific deletion of SRSF2 caused acute liver failure and early death in mice. *Mol. Cell Biol.* **36**, 1628–1638.

Damianov, A., and Black, D.L. (2010). Autoregulation of Fox protein expression to produce dominant negative splicing factors. *RNA* **16**, 405–416.

Das, S., and Krainer, A.R. (2014). Emerging functions of SRSF1, splicing factor and oncoprotein, in RNA metabolism and cancer. *Mol. Cancer Res.* **12**, 1195–1204.

Datta, A., Ghatak, D., Das, S., Banerjee, T., Paul, A., Butti, R., Gorain, M., Ghuwalewala, S., Roychowdhury, A., Alam, S.K., and Das, P. (2017). p53 gain-of-function mutations increase Cdc7-dependent replication initiation. *EMBO Rep.* **18**, 2030–2050.

Ding, J.H., Xu, X., Yang, D., Chu, P.H., Dalton, N.D., Ye, Z., Yeakley, J.M., Cheng, H., Xiao, R.P., Ross, J., and Chen, J. (2004). Dilated cardiomyopathy caused by tissue-specific ablation of SC35 in the heart. *EMBO J.* **23**, 885–896.

Eke, I., Zong, D., Aryankalayil, M.J., Sandfort, V., Bylicky, M.A., Rath, B.H., Graves, E.E., Nussenzweig, A., and Coleman, C.N. (2020). 53BP1/RIF1 signaling promotes cell survival after multifractionated radiotherapy. *Nucleic Acids Res.* **48**, 1314–1326.

El Marjou, F., Janssen, K.P., Chang, B.H., Li, M., Hindie, V., Chan, L., Louvard, D., Chambon, P., Metzger, D., and Robine, S. (2004). Tissue-specific and inducible Cre-mediated recombination in the gut epithelium. *Genesis* **39**, 186–193.

Feng, Y., Valley, M.T., Lazar, J., Yang, A.L., Bronson, R.T., Firestein, S., Coetzee, W.A., and Manley, J.L. (2009). SRP38 regulates alternative splicing and is required for Ca²⁺ handling in the embryonic heart. *Dev. Cell* **16**, 528–538.

Garrido-Martín, D., Palumbo, E., Guigó, R., and Breschi, A. (2018). ggsashimi: sashimi plot revised for browser- and annotation-independent splicing visualization. *PLoS Comp. Biol.* **14**, e1006360.

Gonçalves, V., Matos, P., and Jordan, P. (2009). Antagonistic SR proteins regulate alternative splicing of tumor-related Rac1b downstream of the PI3-kinase and Wnt pathways. *Hum. Mol. Genet.* **18**, 3696–3707.

Graveley, B.R., Brooks, A.N., Carlson, J.W., Duff, M.O., Landolin, J.M., Yang, L., Artieri, C.G., van Baren, M.J., Boley, N., Booth, B.W., and Brown, J.B. (2011). The developmental transcriptome of *Drosophila melanogaster*. *Nature* **471**, 473–479.

Harfe, B.D., Scherz, P.J., Nissim, S., Tian, H., McMahon, A.P., and Tabin, C.J. (2004). Evidence for an expansion-based temporal Shh gradient in specifying vertebrate digit identities. *Cell* **118**, 517–528.

Harris, S.L., and Levine, A.J. (2005). The p53 pathway: positive and negative feedback loops. *Oncogene* **24**, 2899–2908.

Hayakawa-Yano, Y., yeoSuyama, S., Nogami, M., Yugami, M., Koya, I., Furukawa, T., Zhou, L., Abe, M., Sakimura, K., Takebayashi, H., and Nakanishi, A. (2017). An RNA-binding protein, Qki5, regulates embryonic

- neural stem cells through pre-mRNA processing in cell adhesion signaling. *Genes Dev.* **31**, 1910–1925.
- Hu, J.K.H., Du, W., Shelton, S.J., Oldham, M.C., DiPersio, C.M., and Klein, O.D. (2017). An FAK-YAP-mTOR signaling axis regulates stem cell-based tissue renewal in mice. *Cell Stem Cell* **21**, 91–106.e6.
- Jadhav, U., Saxena, M., O'Neill, N.K., Saadatpour, A., Yuan, G.C., Herbert, Z., Murata, K., and Shivdasani, R.A. (2017). Dynamic reorganization of chromatin accessibility signatures during dedifferentiation of secretory precursors into Lgr5+ intestinal stem cells. *Cell Stem Cell* **21**, 65–77.e5.
- Jin, Y., Dong, H., Shi, Y., and Bian, L. (2018). Mutually exclusive alternative splicing of pre-mRNAs, *9* (Wiley Interdiscip. Rev. RNA), p. e1468.
- Jumaa, H., and Nielsen, P.J. (1997). The splicing factor SRp20 modifies splicing of its own mRNA and ASF/SF2 antagonizes this regulation. *EMBO J.* **16**, 5077–5085.
- Jumaa, H., Wei, G., and Nielsen, P.J. (1999). Blastocyst formation is blocked in mouse embryos lacking the splicing factor SRp20. *Curr. Biol.* **9**, 899–902.
- Kalsotra, A., Xiao, X., Ward, A.J., Castle, J.C., Johnson, J.M., Burge, C.B., and Cooper, T.A. (2008). A postnatal switch of CELF and MBNL proteins reprograms alternative splicing in the developing heart. *Proc. Natl. Acad. Sci. USA* **105**, 20333–20338.
- Kanadia, R.N., Clark, V.E., Punzo, C., Trimarchi, J.M., and Cepko, C.L. (2008). Temporal requirement of the alternative-splicing factor Sfrs1 for the survival of retinal neurons. *Development* **135**, 3923–3933.
- Katsuyama, T., Li, H., Comte, D., Tsokos, G.C., and Moulton, V.R. (2019). Splicing factor SRSF1 controls T cell hyperactivity and systemic autoimmunity. *J. Clin. Invest.* **129**, 5411–5423.
- Li, M., Indra, A.K., Warot, X., Brocard, J., Messaddeq, N., Kato, S., Metzger, D., and Chambon, P. (2000). Skin abnormalities generated by temporally controlled RXR α mutations in mouse epidermis. *Nature* **407**, 633–636.
- Manley, J.L., and Krainer, A.R. (2010). A rational nomenclature for serine/arginine-rich protein splicing factors (SR proteins). *Genes Dev.* **24**, 1073–1074.
- McKinley, K.L., Castillo-Azofeifa, D., and Klein, O.D. (2020). Tools and concepts for interrogating and defining cellular identity. *Cell Stem Cell* **26**, 632–656.
- Muzumdar, M.D., Tasic, B., Miyamichi, K., Li, L., and Luo, L. (2007). A global double-fluorescent Cre reporter mouse. *Genesis* **45**, 593–605.
- Ni, J.Z., Grate, L., Donohue, J.P., Preston, C., Nobida, N., O'Brien, G., Shiu, L., Clark, T.A., Blume, J.E., and Ares, M. (2007). Ultraconserved elements are associated with homeostatic control of splicing regulators by alternative splicing and nonsense-mediated decay. *Genes Dev.* **21**, 708–718.
- Nowicka, M., and Robinson, M.D. (2016). DRIMSeq: a Dirichlet-multinomial framework for multivariate count outcomes in genomics. *F1000Res.* **5**, 1356.
- Nusse, Y.M., Savage, A.K., Marangoni, P., Rosendahl-Huber, A.K., Landman, T.A., de Sauvage, F.J., Locksley, R.M., and Klein, O.D. (2018). Parasitic helminths induce fetal-like reversion in the intestinal stem cell niche. *Nature* **559**, 109–113.
- Pan, Q., Shai, O., Lee, L.J., Frey, B.J., and Blencowe, B.J. (2008). Deep surveying of alternative splicing complexity in the human transcriptome by high-throughput sequencing. *Nat. Genet.* **40**, 1413–1415.
- Pandit, S., Zhou, Y., Shiu, L., Coutinho-Mansfield, G., Li, H., Qiu, J., Huang, J., Yeo, G.W., Ares, M., Jr., and Fu, X.D. (2013). Genome-wide analysis reveals SR protein cooperation and competition in regulated splicing. *Mol. Cell* **50**, 223–235.
- Qi, F., Li, Y., Yang, X., Wu, Y.P., Lin, L.J., and Liu, X.M. (2020). Significance of alternative splicing in cancer cells. *Chin. Med. J. (Engl)* **133**, 221–228.
- Salomonis, N., Schlieve, C.R., Pereira, L., Wahlquist, C., Colas, A., Zamboni, A.C., Vranizan, K., Spindler, M.J., Pico, A.R., Cline, M.S., and Clark, T.A. (2010). Alternative splicing regulates mouse embryonic stem cell pluripotency and differentiation. *Proc. Natl. Acad. Sci. USA* **107**, 10514–10519.
- Sanford, J.R., Coutinho, P., Hackett, J.A., Wang, X., Ranahan, W., and Caceres, J.F. (2008). Identification of nuclear and cytoplasmic mRNA targets for the shuttling protein SF2/ASF. *PLoS One* **3**, e3369.
- Schneider, C.A., Rasband, W.S., and Eliceiri, K.W. (2012). NIH image to imageJ: 25 years of image analysis. *Nat. Methods*, 671–675. <https://doi.org/10.1038/nmeth.2089>.
- Seidel, K., Ahn, C.P., Lyons, D., Nee, A., Ting, K., Brownell, I., Cao, T., Carano, R.A., Curran, T., Schober, M., et al. (2010). Hedgehog signaling regulates the generation of ameloblast progenitors in the continuously growing mouse incisor. *Development* **137**, 3753–3761.
- Seidel, K., Marangoni, P., Tang, C., Houshmand, B., Du, W., Maas, R.L., Murray, S., Oldham, M.C., and Klein, O.D. (2017). Resolving stem and progenitor cells in the adult mouse incisor through gene co-expression analysis. *Elife* **6**, e24712.
- Sharir, A., Marangoni, P., Zilionis, R., Wan, M., Wald, T., Hu, J.K., Kawaguchi, K., Castillo-Azofeifa, D., Epstein, L., Harrington, K., and Pagella, P. (2019). A large pool of actively cycling progenitors orchestrates self-renewal and injury repair of an ectodermal appendage. *Nat. Cell Biol.* **21**, 1102–1112.
- Shepard, P.J., and Hertel, K.J. (2009). The SR protein family. *Genome Biol.* **10**, 242.
- Sun, M., Veschi, V., Bagchi, S., Xu, M., Mendoza, A., Liu, Z., and Thiele, C.J. (2019). Targeting the chromosomal passenger complex subunit INCENP induces polyploidization, apoptosis, and senescence in neuroblastoma. *Cancer Res* **79**, 4937–4950.
- Sun, S., Zhang, Z., Sinha, R., Karni, R., and Krainer, A.R. (2010). SF2/ASF autoregulation involves multiple layers of post-transcriptional and translational control. *Nat. Struct. Mol. Biol.* **17**, 306–312.
- Thorne, C.A., Chen, I.W., Sanman, L.E., Cobb, M.H., Wu, L.F., and Altschuler, S.J. (2018). Enteroid monolayers reveal an autonomous WNT and BMP circuit controlling intestinal epithelial growth and organization. *Dev. Cell* **44**, 624–633.e4.
- Varga, J., and Greten, F.R. (2017). Cell plasticity in epithelial homeostasis and tumorigenesis. *Nat. Cell Biol.* **19**, 1133–1141.
- Wang, E.T., Sandberg, R., Luo, S., Khrebtkova, I., Zhang, L., Mayr, C., Kingsmore, S.F., Schroth, G.P., and Burge, C.B. (2008). Alternative isoform regulation in human tissue transcriptomes. *Nature* **456**, 470–476.
- Xu, X., Yang, D., Ding, J.H., Wang, W., Chu, P.H., Dalton, N.D., Wang, H.Y., Bermingham, J.R., Jr., Ye, Z., Liu, F., and Rosenfeld, M.G. (2005). ASF/SF2-regulated CaMKII δ alternative splicing temporally reprograms excitation-contraction coupling in cardiac muscle. *Cell* **120**, 59–72.
- Xu, Y., Zhao, W., Olson, S.D., Prabhakara, K.S., and Zhou, X. (2018). Alternative splicing links histone modifications to stem cell fate decision. *Genome Biol.* **19**, 133.
- Yan, K.S., Gevaert, O., Zheng, G.X.Y., Anchang, B., Probert, C.S., Larkin, K.A., Davies, P.S., Cheng, Z.F., Kaddis, J.S., Han, A., and Roelf, K. (2017). Intestinal enteroendocrine lineage cells possess homeostatic and injury-inducible stem cell activity. *Cell Stem Cell* **21**, 78–90.e6.
- Yeo, G.W., Coufal, N.G., Liang, T.Y., Peng, G.E., Fu, X.D., and Gage, F.H. (2009). An RNA code for the FOX2 splicing regulator revealed by mapping RNA-protein interactions in stem cells. *Nat. Struct. Mol. Biol.* **16**, 130–137.
- Yu, T., Graf, M., Renn, J., Scharlt, M., Larionova, D., Huysseune, A., Witten, P.E., and Winkler, C. (2017). A vertebrate-specific and essential role for osterix in osteogenesis revealed by gene knockout in the teleost medaka. *Development* **144**, 265–271.
- Yu, T., and Klein, O.D. (2020). Molecular and cellular mechanisms of tooth development, homeostasis and repair. *Development* **147**, dev184754.
- Zhang, Y., Chen, K., Sloan, S.A., Bennett, M.L., Scholze, A.R., O'Keefe, S., Phatnani, H.P., Guarnieri, P., Caneda, C., Ruderisch, N., and Deng, S. (2014). An RNA-sequencing transcriptome and splicing database of glia, neurons, and vascular cells of the cerebral cortex. *J. Neurosci.* **34**, 11929–11947.
- Zwick, R.K., Ohlstein, B., and Klein, O.D. (2019). Intestinal renewal across the animal kingdom: comparing stem cell activity in mouse and *Drosophila*. *Am. J. Physiol. Gastrointest. Liver Physiol.* **316**, G313–G322.

STAR★METHODS

KEY RESOURCES TABLE

REAGENT or RESOURCE	SOURCE	IDENTIFIER
Antibodies		
Rabbit Anti-Ameloblastin (M-300) antibody	Santa Cruz Biotechnology	Cat# sc-50534; RRID: AB_2226393
Rat Anti-BrdU antibody	Abcam	Cat# ab6326 ;RRID: AB_305426
Rabbit Anti-Caspase-3, phospho (Cleaved Asp175) antibody	Cell Signaling Technology	Cat# 8202,;RRID: AB_1658166
Rabbit Anti-Survivin antibody	Cell Signaling Technology	Cat# 2808,;RRID: AB_2063948
Rabbit Anti-Phospho-Histone H3 antibody	Cell Signaling Technology	Cat# 9706,;RRID: AB_331748
Rabbit Anti-Cleaved Notch1 (Val1744) (D3B8) antibody	Cell Signaling Technology	Cat# 4147,;RRID: AB_2153348
Rabbit Anti-Olfm4 (D6Y5A) XP® antibody	Cell Signaling Technology	Cat# 39141,;RRID: AB_2650511
Rabbit Anti-Cdc45 (D7G6) antibody	Cell Signaling Technology	Cat# 11881, RRID: AB_2715569
Mouse Anti-P21 antibody	BD Biosciences	Cat# 556431,;RRID: AB_396415
Mouse Anti-Incnp antibody (B-4)	Santa Cruz Biotechnology	Cat# sc-376514,;RRID: AB_11149761
Mouse Anti-Rif1 antibody (B-4)	Santa Cruz Biotechnology	Cat# Sc-515573
Rabbit Anti-P53 antibody	Proteintech	Cat# 10442-1-AP,;RRID: AB_2206609
Rabbit Anti-SRSF1 antibody	Abcam	Cat# ab38017,;RRID: AB_882519
Rabbit Anti-SRSF3 antibody	ProSci	Cat# 8179
Chicken Anti- Green Fluorescent Protein (GFP) Antibody	Aves Lab	Cat# GFP-1020,;RRID: AB_10000240
Chemicals, peptides, and recombinant proteins		
Control AMO	GeneTools	Stand. Control Oligo Cat# (PCO-100)
Oligo: <i>mCdc45</i> E5 ACTGAAAAACAGG ACGAGGCACTGT	GeneTools	Custom Oligo Cat# CO-300
Oligo: <i>Incnp</i> E13 TGTCCCCACCTA GTCGCACCTGTTG	GeneTools	Custom Oligo Cat# CO-300
Oligo: <i>Rif1</i> E32 GGTATTATGCTAGACAGAAGTAGA	GeneTools	Custom Oligo Cat# CO-300
Endo-Porter (PEG)	GeneTools	Cat# OT-EP-PEG-1
Critical commercial assays		
RNAscope 2.5 HD Red detection kit	ACD	Cat#322350
<i>In Situ</i> Cell Death Detection Kit, TMR red	Roche	Cat# 12156792910
TSA Cyanine 3 Tyramide Reagent Pack	Perkin Elmer	Cat# AT704B001EA
VECTASTAIN Elite ABC HRP Kit (Peroxidase, Standard)	Vector Laboratories	Cat # PK-6100
Deposited Data		
Raw and processed RNA-seq data	This paper	GEO: GSE193492
Oligonucleotides		
Primer: <i>Srsf1^{fl/fl}</i> Forward GGGACT AATGTGGGAAGAATG Primer: <i>Srsf1^{fl/fl}</i> Reverse AACCTAA ACTATTGCTCCCATCTG	IDT	Xu et al., 2005
Primer: <i>Srsr31^{fl/fl}</i> Forward GCGCAGGTAAGTGGAGAGA Primer: <i>Srsf3^{fl/fl}</i> Reverse CCCTTTTATTGGTCAGTGA	IDT	Jumaa et al., 1999

(Continued on next page)

REAGENT or RESOURCE	SOURCE	IDENTIFIER
Primer: <i>Cre^{ER}</i> Forward TGGAGATCTTCGACATGCTG Primer: <i>Cre^{ER}</i> Reverse CACGTTCTTGCACCTTCATGC	IDT	JAX
Primer: <i>Cdc45</i> Forward TGTGTGCTTGCAAGATCCTC Primer: <i>Cdc45</i> Reverse ACCCATCACCGTCACTGTCT	IDT	This Paper
Primer: <i>Cttn</i> Forward AGAGAAGCACGAATCCCAGA Primer: <i>Cttn</i> Reverse TCTTGTCCATCCGATCC	IDT	This Paper
Primer: <i>Gak</i> Forward GGAAGAGCAGCAGGACATTC Primer: <i>Gak</i> Reverse GTAGCCCCAGGAGATCAACA	IDT	This Paper
Primer: <i>GAPDH</i> Forward CATGGCCTTCCGTGTTCCCTA Primer: <i>GAPDH</i> Reverse CCTG CTTACCACCTTCTTGAT	IDT	This Paper
Primer: <i>Hnrmpd</i> Forward GACG CCAGTAAGAACGAGGA Primer: <i>Hnrmpd</i> Reverse TCAG GTGTGTCTGGAGAAAGG	IDT	This Paper
Primer: <i>Incenp</i> Forward CGTGAGAGGGTGAACAGAT Primer: <i>Incenp</i> Reverse CTGCTCCTCCGTTCTGTT	IDT	This Paper
Primer: <i>Lsm6</i> Forward TGTGAGCGTTCTGGATCCG Primer: <i>Lsm6</i> Reverse GGATGAACGCATCTCCGTA	IDT	This Paper
Primer: <i>Ncor1</i> Forward GCTCTTTACCAACGGCACAT Primer: <i>Ncor1</i> Reverse GTTGGTCGTGTTGTTGGAAG	IDT	This Paper
Primer: <i>Picalm</i> Forward CTCAGCAGGGGAATAATGA Primer: <i>Picalm</i> Reverse AGAATGTGGCTGTGCAACTG	IDT	This Paper
Primer: <i>Rif1</i> Forward GTGTCTCGTTTGACATCCA Primer: <i>Rif1</i> Reverse GCGTACTCAAATCCCCAATG	IDT	This Paper
Primer: <i>Srrm2</i> Forward ACCTCCCTGTTTGACAGTCG Primer: <i>Srrm2</i> Reverse GGGAGGCTCAGGAGCTATTT	IDT	This Paper
Software and algorithms		
ImageJ	Schneider et al., 2012	https://imagej.nih.gov/ij/
ImageJ Colocalization plugin	ImageJ	https://imagej.nih.gov/ij/plugins/colocalization.html
SPRING Viewer	Klein Lab	https://github.com/AllonKleinLab/SPRING_de
Prism 9	Graphpad software, Inc	N/A
Adobe illustrator 2020	Adobe Computer software company	N/A

RESOURCE AVAILABILITY

Lead Contact and Materials Availability

Further information and requests for resources and reagents should be directed to and will be fulfilled by the Lead Contact, Dr. Ophir Klein (ophir.klein@ucsf.edu). All unique/stable reagents generated in this study are available by contacting the Lead Contact, but we may require a completed Materials Transfer Agreement if there is potential for commercial application.

Data and Code Availability

RNA-seq data have been deposited at GEO and are publicly available as of the date of publication. Accession numbers are listed in the [key resources table](#).

This manuscript did not generate new code.

Any additional information required to reanalyze the data reported in this paper is available from the lead contact upon request.

EXPERIMENTAL MODELS AND SUBJECT DETAILS

Animals

K14Cre^{ER} (Li et al., 2000), *R26^{mT/mG}* (Muzumdar et al., 2007), *VillinCre^{ER}* (El Marjou et al., 2004) and *ShhCre^{ER}* (Harfe et al., 2004), as well as conditional alleles of *Srsf1^{fl/fl}* (Xu et al., 2005) and *Srsf3^{fl/fl}* (Jumaa et al., 1999) mice were housed and genotyped as previously published. Both male and female adult mutant and Cre-negative littermate control mice at 8–10 weeks of age were used for experiments. All experimental procedures involving mice were approved by the Institutional Animal Care and Use Committee (IACUC) and Laboratory Animal Resource Center (LARC) at the University of California, San Francisco, and the mice were handled in accordance with the principles and procedures of the Guide for the Care and Use of Laboratory Animals under the approved protocol AN180876.

METHOD DETAILS

Tamoxifen injection

Tamoxifen (Sigma T5648) was prepared in corn oil at the concentration of 25 mg/ml. Both control and mutant mice, were injected intraperitoneally with 2.5 mg tamoxifen per day per 20 g body weight for two successive days to induce Cre-mediated gene deletion. Animals were euthanized two to six days after tamoxifen injection.

BrdU injection

5-bromo-2'-deoxyuridine (BrdU) (Sigma B9285) was prepared in D-PBS (w/o calcium and magnesium salts) at the concentration of 10 mg/ml. Both control and mutant mice were injected intraperitoneally with a single dose (1 mg) per 20g body weight. Mice were euthanized 30 minutes after BrdU injection. The number of BrdU positive cells was counted for quantitative analyses.

Tissue preparation

Lower mandible

Adult mice were euthanized and perfused with 4% paraformaldehyde (PFA) in PBS. Lower mandibles were dissected from control, *K14^{CreER};Srsf1^{fl/fl}* and *K14^{CreER};Srsf3^{fl/fl}* mutants, and post-fixed in 4% PFA overnight at 4°C. Mandibles were decalcified with 0.5M EDTA for 2 weeks, dehydrated in 70% EtOH, embedded in paraffin and sectioned at 6 μm.

Small intestine

Adult control and *Villin^{CreER};Srsf1^{fl/fl}* mutants were euthanized and perfused with 4% PFA in PBS. The first 10 cm of small intestinal tissues were perfusion-fixed with 4% PFA and post-fixed in 4% PFA overnight at 4°C. Tissues were then dehydrated in 70% EtOH, embedded in paraffin and sectioned at 6 μm.

Immunofluorescence assays

Immunofluorescence staining was performed as previously described (Hu et al., 2017). Additionally, for staining of CASP3, CDC45, NCOR1, NICD, OLFM4, P53, P21, RIF1, SRSF1 and SRSF3, primary antibodies were detected by biotinylated secondary antibodies, and then sequentially amplified using VECTASTAIN Elite ABC HRP Kit (Vector Laboratories) and Tyramide Signal Amplification (Perkin Elmer). All images were acquired with a Leica TCS SP8 X confocal microscope.

TUNEL assay

TUNEL assay was performed using the *In Situ* Cell Death Detection Kit, TMR red (Roche), according to the manufacturer's instructions. The number of TUNEL positive nuclei was counted for quantitative analyses.

Hematoxylin & Eosin (H&E) staining

Adult mouse mandibles were dissected and fixed in 4% PFA overnight at 4°C. Samples were washed, decalcified for 2 weeks and then dehydrated in 70% EtOH. Mandibles were embedded in paraffin and sectioned at 6 μm. H&E staining was performed as previously described (Hu et al., 2017).

Bulk RNA-Seq and analysis

3 control and 4 *K14^{CreER};Srsf1^{fl/fl}* mutant mice were used for RNA extraction. Each RNA sample was isolated from 2 laCLs using the RNeasy mini kit (QIAGEN 74104) according to the manufacturer's instructions. RNA quality was assessed using a Pico Chip on an Agilent 2100 Bioanalyzer (Agilent Technologies). Samples with RNA-integrity (RIN) scores > 8.0 were used by the UCSF Functional Genomics Core. Bulk RNA-Seq was performed on Illumina HiSeq4000 system according to the manufacturer's instructions with paired-end 100bp sequencing type. For each condition, RNA-Seq libraries were prepared with the TruSeq mRNA Kit. RNA-Seq reads were mapped to the reference mouse genome (GRCm38.78). Kallisto (0.44.0) was used to count the number of reads aligned to each transcript. Differential expression analysis was performed using the DESeq2 (v1.16.1) to identify genes that were significantly up- or down-regulated in the *Srsf1* mutant laCL (n=4), relative to controls (n=3). The p-values were adjusted to account for multiple testing with the false discovery rate (FDR) < 0.1. The bulk RNA-Seq data reported in this study will be uploaded upon acceptance of the paper.

Bulk RNA-Seq alternative splicing analysis

JuncBASE (Brooks et al., 2011) was used to identify and quantify AS events. The length-normalized counts for each AS inclusion or exclusion event in each of the sample was obtained from the last step of JuncBASE. The counts were adapted to a format amenable for DRIMSeq (Nowicka and Robinson, 2016), a statistical testing framework. DRIMSeq was used to assign p-values to each AS event. Q-Q plots and volcano plots were output from JuncBASE. The heatmap was plotted using a custom script written with the matplotlib package in python. Sashimi plots for quantitative visualization of sequencing reads aligned to gene annotations were generated using ggsashimi (Garrido-Martín et al., 2018). To identify the potential binding targets of SRSF1, the output list of alternative spliced events from JuncBASE was overlapped with published CLIP tags from 4 papers (Sanford et al., 2008; Pandit et al., 2013; Anczuków et al., 2015), respectively using Venn diagram. 52 overlapping targets were found as putative alternatively spliced binding targets of SRSF1, shown in Table S2. Venn diagrams were made using the matplotlib venn package in python.

Reverse transcription PCR (RT-PCR)

LaCL samples were isolated as previously described (Chavez et al., 2014). DAPI^{low}EpCAM⁺CD44⁺ small intestine crypt epithelial cells were obtained through flow cytometry as previously described (Nusse et al., 2018). RNA samples obtained from control and *K14^{CreER};Srsf1^{fl/fl}* mutant laCL 1 day after tamoxifen injection, as well as control and *Villin^{CreER};Srsf1^{fl/fl}* mutant small intestine crypt epithelial cells 2 days after tamoxifen injection were isolated using GenCatchTM Total RNA miniprep kit (Epoch Life Science 1660050). RNA samples were then reverse-transcribed to cDNA using SensiFASTTM cDNA Synthesis Kit (BioLine BIO-65053). Both steps were performed according to the manufacturer's instructions. RT-PCR were performed using iTAQ CYBR green (Biorad) with the following conditions: 5 minutes at 95°C and 35 cycles of amplification (30 seconds at 95°C, 50 seconds at 60°C and 1 minute at 72°C). The relative changes of transcript expression between controls and *Srsf1* mutants were analyzed by ImageJ as previously described (Yu et al., 2017). In brief, band intensities were first converted into histograms, from which the area under the curve can be measured using the Wand tool and the relative expression between control and mutant samples were calculated. Percent spliced in changes (Δ PSI) were calculated using the band intensity of the inclusion event divided by the band intensity of the inclusion event plus band intensity of the exclusion (i.e., inclusion event/(inclusion + exclusion event)). The primer sets used are listed in the key resources table. All measurements were normalized to GAPDH.

QUANTIFICATION AND STATISTICAL ANALYSIS

Statistical analysis

All of the data points are biological replicates and were replicated at least three times. Bar charts indicate the mean of samples and error bars represent mean \pm SD (standard deviation). *P* value were derived from unpaired two tail Student's t tests, assuming equal variance (**P* < 0.05, ***P* < 0.001, ****P* < 0.001 and n.s. not significant).

ImageJ image analysis

Colocalization of SRSF1, SRSF3, CDC45, RIF1, NCOR1 with DAPI was measured using the ImageJ plugin "Colocalization". Percentage of the immunostained area was detected as previously described in Hu et al., 2017.